Fluid Dynamics of a Terrestrial Magma Ocean

V. S. Solomatov
New Mexico State University

The scenario of crystallization of a terrestrial magma ocean that seems to be consistent with both fluid dynamical and geochemical constraints is as follows. Even the largest impact is unlikely to melt the Earth completely. After the isostatic adjustment the temperatures at the bottom of the mantle were probably near or somewhat above the solidus. In less than a thousand years the solidification front propagates toward the surface and stops at some critical pressure, leaving the mantle below undifferentiated. Differentiation occurs mainly in the remaining shallow magma ocean, the lifetime of which extends well beyond the formation period. Iron delivered by subsequent impacts accumulates at the bottom of this shallow magma ocean and segregates into the Earth's core. This boundary can correspond to the metal-silicate equilibrium pressure of 28 GPa suggested by experiments on fractionation of siderophile elements.

1. INTRODUCTION

A number of arguments suggest that the Earth underwent a substantial melting during the accretion period. In particular, it has been realized that some of the Earth-forming planetesimals were inevitably of the size of Mars or the Moon (*Safronov,* 1978; *Wetherill,* 1985, 1990, 1992; *Weidenschilling et al.,* 1997). Collisions with bodies of this size could melt and even partially vaporize the Earth (*Safronov,* 1978; *Benz and Cameron,* 1990; *Melosh,* 1990). Such large impactors also gave a successful explanation for the origin of the Moon, its composition, and the angular momentum of the Earth-Moon system (*Benz et al.,* 1986, 1987, 1989; *Stevenson,* 1987; *Newsom and Taylor,* 1989; *Canup and Esposito,* 1996; *Ida et al.,* 1997; *Cameron,* 1997; *Canup and Agnor,* 2000). This and other factors such as greenhouse effect, core formation, and radiogenic heating by short-lived isotopes (*Flasar and Birch,* 1973; *Safronov,* 1978; *Kaula,* 1979; *Abe and Matsui,* 1986; *Matsui and Abe,* 1986; *Zahnle et al.,* 1988) imply a significant melting of the early Earth and lead to the hypothesis of a magma ocean.

The magma ocean hypothesis provided a new basis for the explanation of the present-day composition of the Earth (*Ohtani,* 1985; *Ohtani and Sawamoto,* 1987; *Agee and Walker,* 1988; *Herzberg and Gasparik,* 1991; *Gasparik and Drake,* 1995). However, geochemical models of differentiation of a terrestrial magma ocean faced serious limitations imposed by the observed nearly chondritic abundances of minor and trace elements, which forbid any substantial differentiation of perovskite in the lower mantle (*Kato et al.,* 1988a,b; *Ringwood,* 1990; *McFarlane and Drake,* 1990; *McFarlane et al.,* 1994). On the other hand, the partition coefficients are not well constrained at realistic temperatures, pressures, and compositions of magma oceans, and the range of possible scenarios of chemical differentiation is still unclear (e.g., *Presnall et al.,* 1998).

The problem of the apparent excess of siderophile elements in the Earth's mantle also seems to have a solution based on the magma ocean hypothesis. Recent experiments suggest that metal/silicate chemical equilibrium was established around 28 GPa and 2200 K, which can be explained with the help of a core formation model involving a deep magma ocean (*Li and Agee,* 1996; *Righter et al.,* 1997; *Righter and Drake,* 1997). However, the physical nature of this particular pressure remains unclear.

Fluid dynamics provided additional constraints on crystallization of a terrestrial magma ocean (*Tonks and Melosh,* 1990; *Davies,* 1990; *Miller et al.,* 1991a,b; *Abe,* 1993, 1995, 1997; *Solomatov and Stevenson,* 1993a,b,c). It was suggested that a low-viscosity, vigorously convecting magma ocean is more similar to an atmosphere rather than to a solid mantle. Even the temperature distribution is analogous to one of a "wet" atmosphere with condensation and evaporation (equivalent to crystallization and melting).

Important for geochemical implications was the idea of nonfractional (or equilibrium) crystallization as an alternative to the commonly assumed scenario of fractional crystallization. *Tonks and Melosh* (1990) argued that convection can prevent crystal settling so that melting does not necessarily cause differentiation. Further studies by *Solomatov and Stevenson* (1993a) and *Solomatov et al.* (1993) showed that the physics of suspension and differentiation in magma oceans is more complicated. Although crystal settling can be prevented, it is not as easy as was originally thought. It seems that many theories developed for rather simple situations cannot be applied to magma oceans because of the extreme conditions and the diversity of physical processes in magma oceans.

This is particularly true for convection. Early analyses of convection in magma oceans were based on a "classical" model of thermal convection that is applicable only to relatively weak convection. However, a magma ocean is

likely to be in a different convective regime, perhaps "hard" turbulence convection (*Spera*, 1992). Kinetics of crystal nucleation and growth is another example of a poorly understood process. It controls the size of crystals and therefore the rate of differentiation.

The goal of this chapter is to review the physical processes in a terrestrial magma ocean and suggest a scenario of crystallization of the molten Earth that is consistent with geochemical constraints.

2. THERMODYNAMICS

Thermodynamics of a partially molten mantle is affected by phase changes and can be constructed with the help of a standard thermodynamic approach (*Ghiorso*, 1997; *Asimow et al.*, 1997). The phase diagram of the upper mantle shown in Fig. 1 is calculated with the help of a three-component model of magma oceans described by *Solomatov and Stevenson* (1993b). We assume that at P < 10 GPa the three components olivine, clinopyroxene, and orthopyroxene form a eutectic-like system. Variation of melt fraction between liquidus and solidus for this model is given in Fig. 2 along with the experimental data from *McKenzie and Bickle* (1988). Since the Earth's mantle is not ideal, the melting temperatures, their gradients, and the fractions of the three components are adjusted to fit the experimental data shown in Figs. 1 and 2.

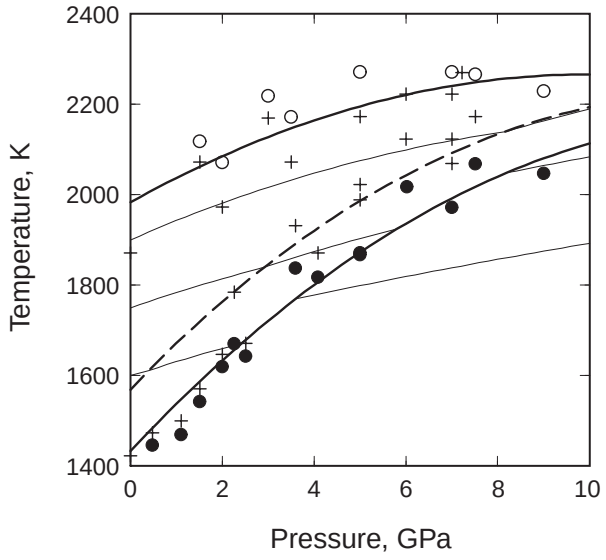

Fig. 1. Three adiabats in the upper mantle are shown with thin solid lines starting at 1600, 1750, and 1900 K. Liquidus, solidus (heavy solid lines), and the beginning of crystallization of orthopyroxene (dashed line) are shown together with experimental data for peridotites from *McKenzie and Bickle* (1988), *Scarfe and Takahashi* (1986), and *Ito and Takahashi* (1987): liquid (open circles), solid (solid circles), and partial melt (crosses).

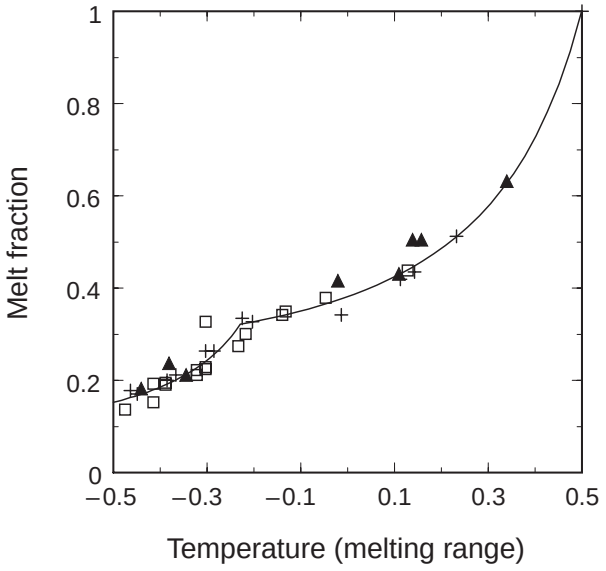

Fig. 2. Variation of melt fraction between liquidus (T = –0.5) and solidus (T = 0.5) suggested by our model (solid line) fits well the experimental data collected by *McKenzie and Bickle* (1988): 0 ≤ P ≤ 0.5 GPa (crosses), 0.5 ≤ P 1.5 (squares), 1.5 < P (triangles). This is a typical three-component eutectic-like system (olivine-orthopyroxene-clinopyroxene) with a step-like melting at the solidus. Solid solutions would replace this jump by a steep gradient.

In vigorously convecting systems such as magma oceans the temperature distribution is nearly adiabatic and isentropic

$$\frac{dT}{dP} = \frac{\alpha T}{\rho c_p} \qquad (1)$$

where T is the temperature, P is the pressure, α is the coefficient of thermal expansion, c_p is the isobaric heat capacity, and ρ is the density. Adiabats starting at different potential temperatures (potential temperature is the adiabatic temperature at P = 0) are shown in Fig. 1.

The three components in the lower mantle are perovskite, $MgSiO_3$, periclase, MgO, and wüstite, FeO. Perovskite has only a small amount of Fe and is considered to be a pure $MgSiO_3$, while periclase and wüstite are assumed to form an ideal solid solution. Figures 3a and 3b show the melting temperatures of $MgSiO_3$, MgO, and FeO, liquidus, solidus, and the adiabats for the lower mantle. The melting temperatures of $MgSiO_3$, MgO, and FeO (Fig. 3a) are based on laboratory experiments and extrapolation to high pressures by *Boehler* (1992) and *Zerr and Boehler* (1993, 1994).

The liquidus and solidus curves predicted by this model for the lower mantle are significantly steeper than single-phase adiabats. The solidus is very close to one estimated by *Holland and Ahrens* (1997) and *Zerr et al.* (1998). The liquidus is high compared to previously published estimates because of the high melting temperature of perovskite and the assumption that perovskite forms eutectic-like subsystems with periclase and wüstite. *Abe* (1997), for instance,

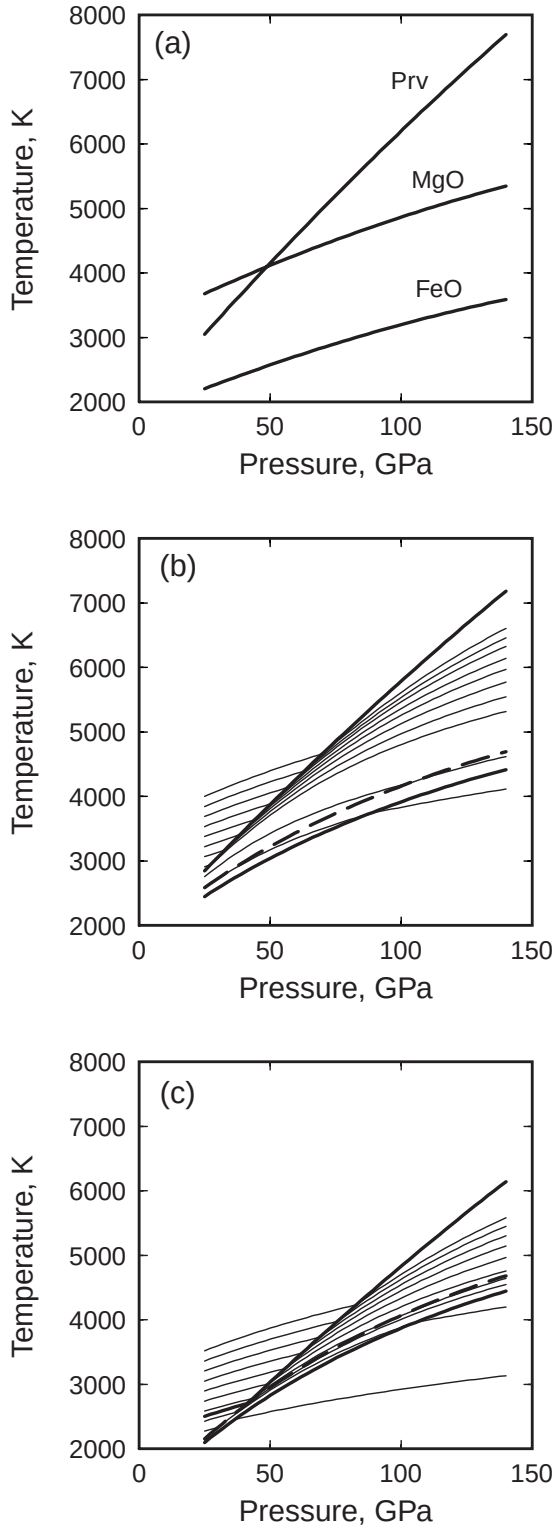

Fig. 3. **(a)** Melting curves of perovskite, MgO, and FeO according to *Boehler* (1992) and *Zerr and Boehler* (1993, 1994). **(b)** Adiabats in the convective magma ocean. Liquidus and solidus are shown with a heavy solid line. The beginning of magnesiowüstite crystallization is shown with a dashed line. **(c)** An example of calculations where magnesiowüstite is the first liquidus phase at the top of the lower mantle as observed by *Agee* (1990) and *Zhang and Herzberg* (1994).

assumed an ideal mixture of $MgSiO_3$ and MgO, while *Miller et al.* (1991b) and *Solomatov and Stevenson* (1993b) assumed a low melting temperature of perovskite based on the data by *Knittle and Jeanloz* (1989). For an ideal eutectic-like system, the liquidus T_{liq} approximately follows the melting temperature T_{prv} of pure perovskite $MgSiO_3$ lowered by the presence of MgO and FeO

$$T_{prv} - T_{liq} \approx \frac{k_B}{\Delta S_{prv}} n_{mw} T_{prv} \tag{2}$$

where ΔS_{prv} is the entropy change per atom upon melting of pure perovskite, and n_{mw} is the molar fraction of magnesiowüstite. For $n_{mw} \approx 0.3$, $\Delta S_{prv} \approx 5\ k_B$ [assuming that the entropy change is approximately k_B per atom (*Stishov,* 1988)] and $T_{prv} \approx 7500$ K we obtain $T_{prv} - T_{liq} \approx 450$ K.

Agee (1990) and *Zhang and Herzberg* (1994) found that magnesiowüstite is the liquidus phase in both chondrites and peridotites just slightly below the upper mantle/lower mantle boundary. A small fraction of Fe in the solid perovskite and the presence of other components (e.g., Ca-perovskite) in melt would decrease the liquidus temperature. The estimates of the entropy change are also not very accurate. As a result, magnesiowüstite can be the first liquidus phase at low pressures, although at higher pressures it would still be substituted by perovskite (Fig. 3c).

3. FORMATION OF MAGMA OCEANS BY GIANT IMPACTS

3.1. Mantle Temperature Before Impacts

It is quite common to assume that at the latest stages of Earth's formation the mantle temperature is close to solidus (*Abe and Matsui,* 1986; *Sasaki and Nakazawa,* 1986; *Zahnle et al.,* 1988). However, since the mantle solidus is steeper than the adiabat in the solid mantle, such temperature distribution is gravitationally unstable. The effective density contrast between the upper and lower parts of the mantle is

$$\Delta\rho \approx \frac{1}{2}\alpha\rho H\left(\frac{dT_{sol}}{dz} - \frac{dT_{ad}}{dz}\right) \approx 120\ \text{kg m}^{-3} \tag{3}$$

where (see Table 1) $\rho = 4000$ kg m^{-3}, $\alpha \approx 3 \times 10^{-5}$ K^{-1}, $H \approx 3 \times 10^6$ m is the thickness of the mantle, dT_{sol}/dz is the solidus gradient, and dT_{ad}/dz is the adiabatic gradient (Fig. 3). This density contrast causes gravitational instability that is somewhat similar to a classical Rayleigh-Taylor instability in a two-layer system. The timescale for the overturn can then be estimated as (*Turcotte and Schubert,* 1982)

$$t_{RT} \approx 26\frac{\eta_s}{\Delta\rho g H} \tag{4}$$

where η_s is the viscosity and g is the gravity.

TABLE 1. "Typical" values of physical parameters for a magma ocean in the early stages of crystallization (lower mantle, the liquidus phase is perovskite).

Density, ρ	4×10^3 kg m^{-3}
Temperature, T	4×10^3 K
Thermal expansion, α	5×10^{-5} K^{-1}
Thermal capacity, c_p	10^3 J kg^{-1} K^{-1}
Gravity, g	10 m s^{-2}
Crystal/melt density difference, $\Delta\rho$	300 kg m^{-3}
Viscosity of melt at the liquidus, η_l	0.1 Pa s
Viscosity of solids above the solidus, η_s	10^{17} Pa s
Diffusion coefficient, D	10^{-9} m^2 s^{-1}
Enthalpy change upon melting, ΔH	10^6 J kg^{-1}
Apparent surface energy, σ_{app}	0.02 J m^{-2}
Pre-factor in the nucleation rate, a	10^{20} m^{-3} s^{-1}
Liquidus gradient, dT_l/dz	2×10^{-3} K m^{-1}
Adiabatic gradient, dT_{ad}/dz	6×10^{-4} K m^{-1}
Variation of liquidus with ϕ, $dT_l/d\phi$	10^3 K
Heat flux, F	10^6 J m^{-2} s^{-1}
Angular velocity, Ω	10^{-4} s^{-1}
Length scale, H	3×10^6 m
Convective velocity, u_0	10 m s^{-1}
Timescale for Ostwald ripening, t	10^6 s
Effective cooling rate in plumes, $\dot{T}$	0.2 K s^{-1}
Crystal size, d	10^{-3} m

This timescale depends critically on η_s. The present-day mantle viscosity is around 10^{22} Pa s (*King*, 1995). For the viscosity $\eta_s \approx 10^{20}$ Pa s corresponding to 200 K hotter mantle (the viscosity decreases roughly at the rate of one order of magnitude per 100 K)

$$t_{RT} \approx 2 \times 10^4 \left(\frac{\eta_s}{10^{20}\ \text{Pa s}} \right) \text{yr} \qquad (5)$$

This is very fast compared to the timescale of Earth's formation, which is of the order of 10^8 yr as suggested by numerical simulations (*Wetherill*, 1990) and by isotopic constraints on the timing of the core formation (*Lee and Halliday*, 1995; *Halliday et al.*, 1996). In fact, a superadiabatic temperature gradient of only 100–200 K over the entire mantle would be eliminated within 10^5 yr or so. Therefore, the mantle had enough time to maintain a nearly adiabatic temperature during the accretion period. However, the situation can be more complicated if a sufficiently large density gradient was established due to crystal/melt differentiation or migration of liquid iron diapirs (*Elsasser*, 1963; *Stevenson*, 1981, 1990; *Karato and Murthy*, 1997a). In particular, an increase of the viscosity with depth could cause a higher concentration of liquid diapirs in high-viscosity regions and make a near-solidus mantle gravitationally stable. On the other hand, if the viscosity variations were small, liquid diapirs could stir the mantle and maintain its nearly adiabatic state. The answer depends on the poorly constrained rheological stratification of the growing Earth.

3.2. Impact-induced Melting

Simulations of impacts (*Melosh*, 1990; *Tonks and Melosh*, 1993; *Pierazzo et al.*, 1997) suggest that the impact completely melts a region with the radius of about half the radius of the Earth. The temperature increase in the remaining part of the Earth is due to the shock wave. It decays very rapidly with the distance from the molten region so that the opposite side of the Earth is heated very little. The gravitational energy associated with this buoyant blob of partially molten material is converted into the heat during the subsequent isostatic adjustment. This process redistributes the mass to form a gravitationally stable system. The flow of solid, dense material replaces the melt, which eventually moves on top of the solid or partially molten layers. The gravitational energy released during viscous deformation results in an additional temperature increase of 300–400 K on average (*Tonks and Melosh*, 1990). A somewhat smaller amount of energy comes from gravitational separation of Fe from the impactor (*Tonks and Melosh*, 1992). The opposite side of the Earth was probably heated by only about 500 K or so due to the net effect of the shock-wave heating, isostatic adjustment, and segregation of Fe from the impactor. If the initial thermal state was adiabatic, then a significant portion of the Earth remained solid. If, however, the initial temperature distribution was close to solidus, then the impact would produce a completely molten region and partially molten region of comparable sizes. In any case, a complete melting of the mantle is unlikely because of the high liquidus temperature.

The stresses ~ $\Delta\rho gR$ associated with the molten blob located on one side of the Earth are on the order of 10 GPa. This exceeds the ultimate strength of rocks, which is about 1–2 GPa (*Davies*, 1982). Therefore, isostatic adjustment could be an extremely fast process. Crystallization is a much slower process that starts effectively at the latest stages of the isostatic adjustment.

4. VISCOSITY OF MAGMA AND "RHEOLOGICAL TRANSITION"

A large degree of melting of the mantle implies a very small viscosity of the magma ocean. Experimental and theoretical studies suggest that the viscosity of many near-liquidus ultramafic silicates at low pressures is around $\eta_l \sim$ 0.1 Pa s (*Bottinga and Weill*, 1972; *Shaw*, 1972; *Persikov et al.*, 1990; *Bottinga et al.*, 1995). Molecular dynamic simulations of MgO-SiO_2 give a value of 3×10^{-3}–5×10^{-3} Pa s at 5 GPa (*Wasserman et al.*, 1993a,b), which is almost independent of temperature and composition.

The viscosity of a completely depolymerized melt weakly increases with pressure (*Andrade*, 1952; *Gans*, 1972). An increase of less than one order of magnitude can be expected along the liquidus throughout the lower mantle. Thus, the viscosity of magma oceans near the liquidus is probably around 10^{-2}–10^{-1} Pa s. In the region between solidus and liquidus it is somewhat higher because of lower

temperatures. However, the temperature effect is small for low-viscosity liquids (<1 Pa s), which exhibit a power-law rather than Arrhenius behavior (*Bottinga et al.,* 1995). The value of 10^{-1} Pa s with the uncertainty of a factor of 10 will be assumed in all subsequent estimates (Table 1).

Many authors pointed out that magma oceans can contain substantial amounts of water (*Holloway,* 1988; *Ahrens,* 1992; *Righter et al.,* 1997). Although water reduces the viscosity of magmas, in the limit of high temperatures the viscosities and diffusivities of many liquids including water are very similar (*Persikov et al.,* 1990). Therefore, the viscosity of completely depolymerized, high-temperature hydrous magma cannot be much different from that of anhydrous magma.

The viscosity of a melt/crystal mixture jumps abruptly near a critical crystal fraction as suggested by theoretical and experimental studies of concentrated suspensions (*Mooney,* 1951; *Roscoe,* 1952; *Brinkman,* 1952; *Krieger and Dougherty,* 1959; *Murray,* 1965; *Frankel and Acrivos,* 1967; *McBirney and Murase,* 1984; *Cambell and Forgacs,* 1990) and by experiments with partial melts (*Arzi,* 1978; *van der Molen and Paterson,* 1979; *Lejeune and Richet,* 1995). This can be called a "rheological transition." It depends on the crystal size distribution, the crystal shape, and other factors and is around 60%.

5. CONVECTION

5.1. "Classical" Model of Turbulent Convection

At small viscosities of the magma ocean, before the rheological transition, convection is extremely turbulent and is driven by cooling from the surface. The convective velocity scales as (*Priestly,* 1959; *Kraichnan,* 1962)

$$u_0 \approx 0.6\left(\frac{\alpha g l F}{\rho c_p}\right)^{1/3} \tag{6}$$

where F is the surface heat flux, l is the mixing length, and the coefficient in front of this equation is constrained by laboratory experiments (*Deardorff,* 1970; *Willis and Deardorff,* 1974) and atmospheric measurements (*Caughey and Palmer,* 1979). The mixing length is approximately equal to the depth of the magma ocean $l \sim H$. For either one-phase values of the parameters given in Table 1 or two-phase values (*Solomatov and Stevenson,* 1993b), $u_0 \approx 4$ m/s.

It is interesting that the parameter $(F/\rho)^{1/3}$ is almost the same for the magma ocean and the atmosphere. This explains why the above estimate is very similar to the observed velocities in the convective boundary layer in the atmosphere (*Caughey and Palmer,* 1979).

5.2. "Hard" Turbulence

At very high Rayleigh numbers (such as those relevant to magma oceans) convection changes to a regime sometimes called "hard" turbulence convection (*Castaing et al.,* 1989; *Shraiman and Siggia,* 1990; *Grossman and Lohse,* 1992; *Siggia,* 1994). By contrast, the ordinary turbulence is called "soft" turbulence. One of the important features of "hard" turbulence convection is the existence of a large-scale circulation ("wind"). The equations suggested by *Shraiman and Siggia* (1990) can be rewritten in the form similar to equation (6)

$$u_0 \approx a\left(\frac{\alpha g l F}{\rho c_p}\right)^{1/3} \tag{7}$$

where the coefficient a is calculated as

$$a \approx \frac{0.052}{0.22^{1/3}}\, x^* \tag{8}$$

where 0.22 and 0.052 are the pre-factors in the scaling relationships for Nusselt and Reynolds numbers correspondingly, and x* is related to u_0 through

$$x^* = 2.5 \ln\left[\frac{\rho u_0 l}{\eta}\frac{1}{x^*}\right] + 6 \tag{9}$$

The solution to the above transcendental equations gives $a \approx 5.9$, which varies weakly with $\rho u_0 l/\eta$.

In the "hard" turbulence regime, the velocity increases by a factor of 10. This brings the estimate of the convective velocity in the magma ocean up to 40 m/s. At even higher Rayleigh numbers, convection was expected to enter a new regime of turbulent convection (*Kraichnan,* 1962; *Siggia,* 1994). However, recent experiments did not show any evidence of such an "ultrahard" regime, and "hard" turbulence was suggested to be the truly asymptotic regime of thermal convection (*Glazier et al.,* 1999). Therefore, "hard" turbulence convection is probably applicable to the extreme conditions of magma oceans.

5.3. Effect of Rotation

Despite recent attempts to study "hard" turbulence in the presence of rotation (*Julien et al.,* 1996), there is no velocity scaling in this case. The problem has not been completely solved yet even for "soft" turbulence. However, the length scale

$$l \sim \frac{u_0}{\Omega} \tag{10}$$

explains rather well the experimentally observed reduction in the convective velocity (*Golitsyn,* 1980, 1981; *Hopfinger et al.,* 1982; *Hopfinger,* 1989; *Boubnov and Golitsyn,* 1986, 1990; *Chen et al.,* 1989; *Fernando et al.,* 1991; *Solomatov and Stevenson,* 1993a). Applying this scaling to "hard" turbulence convection we obtain

$$u_0 \approx 14\left(\frac{\alpha g F}{\rho c_p \Omega}\right)^{1/2} \tag{11}$$

This gives velocities around 16 m/s with the uncertainty of a factor of 3. A moderate value of 10 m/s is used in the estimates below (Table 1).

6. HEAT FLUX

In the early stages of crystallization, when the surface temperature is high, the atmosphere is presumably a "silicate" one (*Thompson and Stevenson,* 1988) and the heat flux can be calculated with the help of the blackbody model

$$F_r = \sigma_B T_s^4 \tag{12}$$

where T_s is the surface temperature and $\sigma_B = 5.67 \times 10^{-8}$ J m^{-2} K^{-4} is the Stefan-Boltzmann constant.

This heat flux must match the heat flux transported to the surface by convection. The convective heat flux depends on whether convection is in the regime of "soft" turbulence or "hard" turbulence. In the "soft" turbulence regime

$$F_{soft} = 0.089 \frac{k(T - T_s)}{H} Ra^{1/3} \tag{13}$$

where

$$Ra = \frac{\alpha g (T - T_s) H^3}{\kappa \nu} \tag{14}$$

is the Rayleigh number, T is the potential temperature, k is the coefficient of thermal conductivity, $\kappa = k/\rho c_p$ is the coefficient of thermal diffusivity, and $\nu = \eta/\rho$ is the kinematic viscosity (*Kraichnan,* 1962; *Siggia,* 1994).

In the "hard" turbulence regime (*Shraiman and Siggia,* 1990; *Siggia,* 1994)

$$F_{hard} = 0.22 \frac{k(T - T_s)}{H} Ra^{2/7} Pr^{-1/7} \lambda^{-3/7} \tag{15}$$

where $Pr = \nu/\kappa$ is the Prandtl number and λ is the aspect ratio for the mean flow. The exact value of λ is unknown for spherical geometry but is probably of the order of unity.

Figure 4 shows that during the initial period of crystallization, when the temperature of the magma ocean is high and convection is in the "hard" turbulence convection regime, the heat flux is close to 10^6 W m^{-2}. During the latest stages of crystallization (upper mantle) the surface temperature drops below 1500 K and the heat flux decreases to 10^2–10^3 W m^{-2} due to a greenhouse effect (*Abe and Matsui,* 1986; *Zahnle et al.,* 1988; *Kasting,* 1988). In the "hard" turbulence regime and for $\eta_l = 0.1$ Pa s this does not happen until almost a complete crystallization of the magma ocean.

7. CONDITIONS FOR EQUILIBRIUM CRYSTALLIZATION

7.1. "Sufficient" Condition for Equilibrium Crystallization

In this section we are concerned with the early crystallization of the magma ocean, before the crystal fraction reaches the rheological transition.

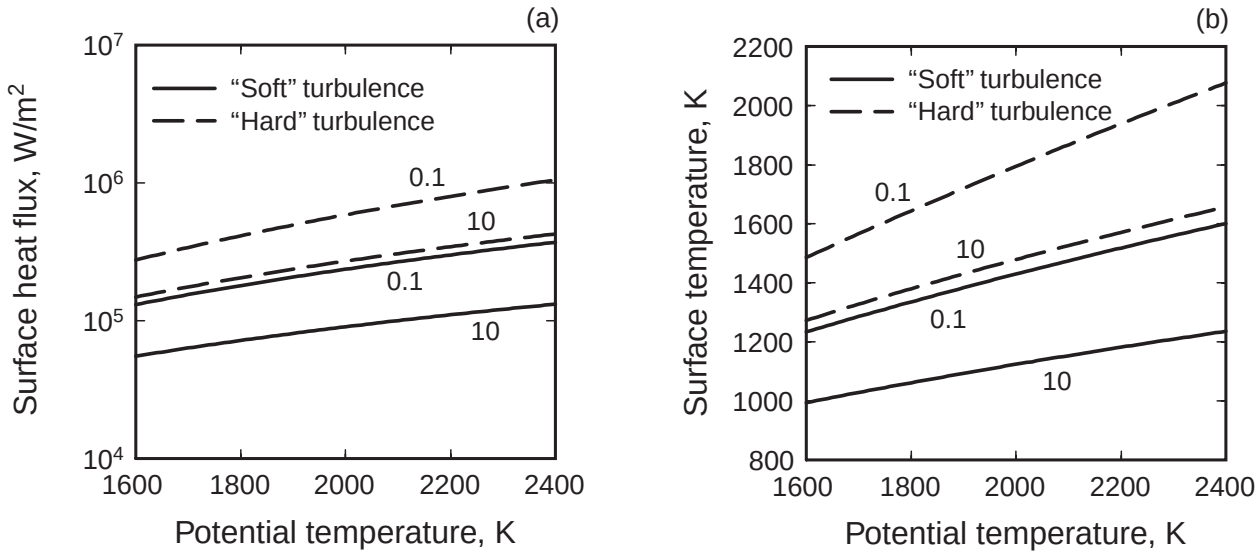

Fig. 4. **(a)** Surface heat flux and **(b)** surface temperature are shown as functions of the potential temperature, the convective regime ("soft" vs. "hard" turbulence), and the viscosity of magma (0.1–10 Pa s).

The simplest scenario in which a magma ocean can crystallize without differentiation is one in which the crystal size and settling velocity are so small that the magma ocean freezes before any crystal-melt segregation occurs. What is the critical crystal size for this to happen?

The crystallization time is around

$$t_{cr} \approx \frac{(\Delta H\phi + c_p \Delta T)M}{FA} \approx 400\,\text{yr} \tag{16}$$

where $\Delta T \sim 1000$ K is the average temperature drop upon crystallization of the magma ocean up to the crystal fraction $\phi \sim 60\%$, M is the mass of the mantle, and s is the surface area of the Earth.

The timescale for crystal settling is (*Martin and Nokes*, 1988, 1989)

$$t_s \approx H/u_s \tag{17}$$

where

$$u_s = f_\phi \frac{\Delta\rho g d^2}{18\eta_l} \tag{18}$$

is the settling velocity and f_ϕ is a hindered settling function such that $f_\phi = 1$ at $\phi = 0$ (*Davis and Acrivos*, 1985). For $\phi \sim 30\%$ (on average) $f_\phi \sim 0.15$.

Requiring that crystallization is faster than settling, that is $t_{cr} < t_s$, we find that the crystal size should be smaller than

$$d_1 = \left(\frac{18H\eta_l}{f_\phi g \Delta\rho t_{cr}}\right)^{1/2} \tag{19}$$

or

$$d_1 \approx 10^{-3}\left(\frac{\eta_l}{0.1\,\text{Pa s}}\right)^{1/2}\left(\frac{F}{10^6\,\text{W m}^{-2}}\right)^{1/2}\text{m} \tag{20}$$

7.2. "Necessary" Condition for Equilibrium Crystallization

The presence of crystals can suppress convection and slow down cooling of the magma ocean as a result of viscous heating and density stratification associated with crystal settling. This happens if the crystal size is larger than (*Solomatov and Stevenson*, 1993a)

$$d_2 = \left(\frac{18\alpha\eta_l F}{f_\phi g c_p \Delta\rho^2 \phi}\right)^{1/2} \tag{21}$$

where f_ϕ is the same as in equation (18).

We obtain

$$d_2 \approx 10^{-3}\left(\frac{\eta_l}{0.1\,\text{Pa s}}\right)^{1/2}\left(\frac{F}{10^6\,\text{W m}^{-2}}\right)^{1/2}\text{m} \tag{22}$$

7.3. Critical Crystal Size for Equilibrium Crystallization

Since both "necessary" and "sufficient" conditions approximately coincide, the critical crystal size for equilibrium crystallization up to about 60% crystal fraction is

$$d_{crit} \approx 10^{-3}\left(\frac{\eta_l}{0.1\,\text{Pa s}}\right)^{1/2}\left(\frac{F}{10^6\,\text{W m}^{-2}}\right)^{1/2}\text{m} \tag{23}$$

The fact that these two estimates are very close to each other is not surprising; their ratio scales approximately as

$$\frac{d_1}{d_2} \sim \left(\frac{\Delta\rho/\rho}{\alpha T}\frac{c_p}{\Delta S}\right)^{1/2} \sim 1 \tag{24}$$

The interval between d_1 and d_2 is negligible compared to the uncertainties in the crystal size. Therefore, consideration of reentrainment of crystals from the bottom (*Tonks and Melosh*, 1990; *Solomatov and Stevenson*, 1993a; *Solomatov et al.*, 1993) is unnecessary for these order-of-magnitude estimates; at $d < d_1$ settling is negligible and reentrainment is unimportant, while at $d > d_2$ convection is suppressed and reentrainment cannot occur.

8. HOW BIG ARE THE CRYSTALS IN MAGMA OCEANS?

8.1. Overview

In general, if the crystal fraction is ϕ and the total number of crystals per unit volume is N then the crystal diameter (assuming spherical shape) is

$$d = \left(\frac{6\phi}{\pi N}\right)^{1/3} \tag{25}$$

The initial number of crystals N per unit volume is controlled by the nucleation process in the downgoing flow. If the number of crystals N does not change with time, then the crystals grow simply because the equilibrium crystal fraction ϕ increases with depth along the adiabat. However, dissolution of smaller crystals and growth of larger crystals decreases N (Ostwald ripening) and increases the average size of crystals according to equation (25). Below we compare two end-member cases: nucleation controlled crystal size (negligible Ostwald ripening) and Ostwald ripening controlled crystal size.

8.2. Crystal Size Controlled by Nucleation

When the downgoing convective flow enters the two-phase region, formation of crystals proceeds via nucleation and growth mechanism (Figs. 5 and 6). This is very similar to bulk crystallization of continuously cooling liquids. In both cases the number of nuclei formed depends on the

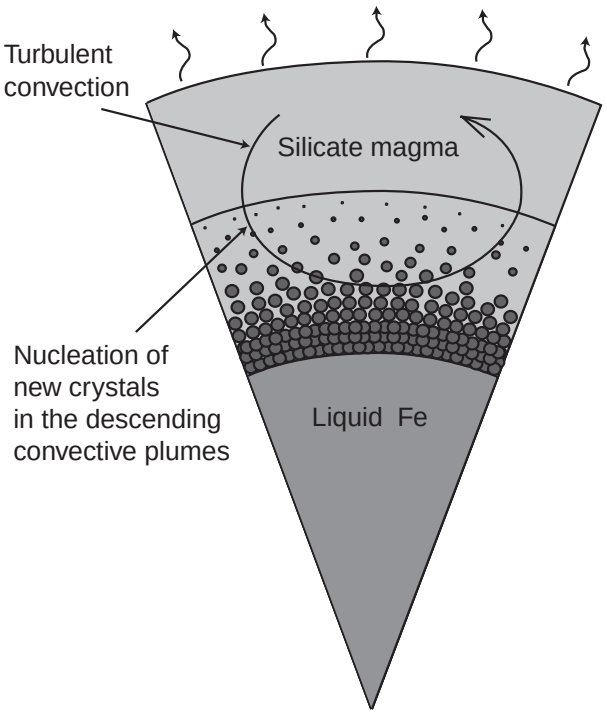

Fig. 5. Magma ocean in the beginning of crystallization. The size of crystals is determined by the number of nuclei produced in the descending plumes upon entering the two-phase region.

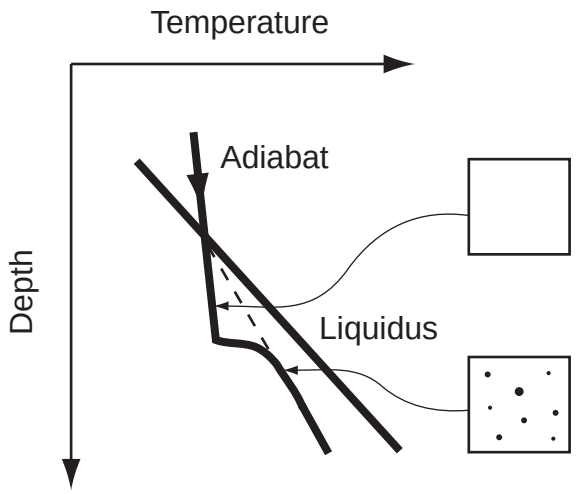

$$\dot{T} = \left(\nabla T_{liq} - \nabla T_{ad}\right) u_0$$

Fig. 6. Nucleation in descending flow in the magma ocean. The temperature in the superliquidus descending flow follows a one-phase adiabat (in an ideal equilibrium, the temperature would follow the two-phase adiabat shown with a dashed line). When the adiabatic temperature drops below liquidus, the temperature keeps following the one-phase adiabat. Nucleation starts after a small metastable overshoot and the temperature quickly approaches the two-phase adiabat.

cooling rate $\dot{T}$. *Solomatov and Stevenson* (1993c) solved this problem for interface kinetics controlled growth. Further analysis (*Solomatov,* 1995) showed that diffusion-controlled growth during nucleation is more consistent with various experimental data on silicates and alloys (Fig. 7), although the effect of transient nucleation (*Kashchiev,* 1969) still needs to be investigated.

The number of nuclei produced per unit volume during the nucleation period is

$$N = 0.2\frac{\zeta^{3/2}\dot{T}^{3/2}p^{3/2}}{A\left|dT_l/d\phi\right|D^{3/2}} \tag{26}$$

where D is the diffusion coefficient, $\zeta = \Delta T/\Delta C$ determines the relationship between the supersaturation ΔC and the supercooling ΔT and is of the order of the difference between liquidus and solidus temperatures, $\zeta \sim T_l - T_s$, A is the coefficient in the nucleation rate function

$$J(\Delta T) = a\exp\left(-\frac{A}{T'^2}\right) \tag{27}$$

$$A = \frac{16\pi\sigma_{app}^3 T_0^2}{3k_B T\rho^2\Delta H^2} \tag{28}$$

where T' is the supercooling, a is a constant, T_0 is the melting temperature of the crystallizing phase, k_B is Boltzmann's constant, ΔH is the enthalpy change per unit mass upon melting, and σ_{app} is the apparent surface energy.

The parameter p in equation (26) is nearly constant (~30). It can be found from

$$p = \ln\left[\frac{6.05\left|dT_l/d\phi\right|aA^{3/2}D^{3/2}}{\zeta^{3/2}\dot{T}^{5/2}p^3}\right] \tag{29}$$

Note that because of a large value of the logarithm, p is insensitive to the uncertainties in the parameters in the above equation.

The effective cooling rate of an adiabatically descending plume (the rate of change of the difference between the liquidus temperature T_l and the actual temperature T_{ad}) is

$$\dot{T} = u_0\left(\frac{dT_l}{dz} - \frac{dT_{ad}}{dz}\right) \tag{30}$$

where dT_l/dz is the liquidus gradient and dT_{ad}/dz is the adiabatic gradient.

From equations (25) and (26) with $\phi \sim 60\%$ we estimate

$$d_{nuc} \approx 3\times10^{-4}\left(\frac{\sigma_{app}}{0.02\ \mathrm{J\ m^{-2}}}\right)\left(\frac{D}{10^{-9}\ \mathrm{m^2\ s^{-1}}}\right)^{1/2}\left(\frac{u_0}{10\ \mathrm{m\ s^{-1}}}\right)^{-1/2}\ \mathrm{m} \tag{31}$$

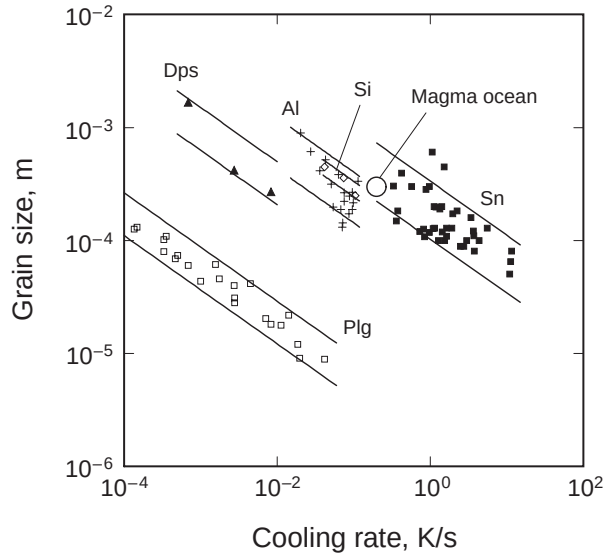

Fig. 7. Crystal size vs. cooling rate for five crystallizing phases (from *Solomatov,* 1995): Sn (from Sn-Pb melt, solid boxes), Al (from Al-Cu melt, pluses), Si (from Al-Si melt, diamonds), diopside (from diopside-plagioclase melt, solid triangles), and plagioclase (from diopside-plagioclase, open boxes), which is a solid solution between albite and anorthite. The data are from *Lofgren et al.* (1974), *Flemings et al.* (1976), *Grove and Walker* (1977), *Walker et al.* (1978), *Ichikawa et al.* (1985), *Grove* (1990), *Smith et al.* (1991), and *Cashman* (1993). The theoretical fit to each dataset consists of two curves showing the range of uncertainties. The curves depend only on one fitting parameter, the apparent surface energy. The location of the magma ocean is shown with a large circle (for the parameters given in Table 1).

It should be emphasized that the value of the surface energy, σ_{app}, is not well constrained. It is not the normal surface energy but rather an apparent one for nucleation. The value of 0.02 J m^{-2} (Table 1) is based on the analogy with some simple cases that suggest a value of σ_{app}, which is almost 1 order of magnitude smaller compared to the usual one (*Dowty,* 1980; *Solomatov,* 1995). It is subject to large uncertainties when extrapolating to magma oceans. The presence of water reduces σ_{app} and increases the nucleation rates (*Fenn,* 1977; *Swanson,* 1977; *Dowty,* 1980; *Davis et al.,* 1997) while only slightly increasing D (at high temperatures it is almost the same for all liquids). Therefore, the presence of water might decrease the crystal size, which is somewhat counterintuitive since one would expect an enhanced crystal growth in the presence of water.

8.3. Crystal Size Controlled by Ostwald Ripening

A simple estimate of the crystal size d_{ost} due to Ostwald ripening can be obtained from diffusion controlled growth (if interface kinetics is the rate-limiting process then the crystal size will be reduced further). In this case (*Lifshitz and Slyozov,* 1961; *Voorhees,* 1992)

$$d_{ost}^3 - d_0^3 = \frac{32}{9} b_\phi \alpha_0 Dt \qquad (32)$$

where d_0 is the initial crystal size, $\alpha_0 = \sigma c_\infty v_m/2RT$, σ is the surface energy, c_∞ is the equilibrium concentration of the crystallizing mineral in the melt, v_m is the molar volume of the crystallizing mineral, t is the characteristic residence time in the two-phase region (~H/u_0), and b_ϕ is a correction to the original *Lifshitz and Slyozov's* (1961) equation for large ϕ such that $b_\phi = 1$ at very small ϕ and $b_\phi \approx 3$ for $\phi \approx 30\%$. Neglecting the initial crystal size we obtain

$$d_{ost} \approx 4 \times 10^{-4} \text{m} \qquad (33)$$

This crystal size is about the same as the one controlled by nucleation (equation (31)).

When the completely molten layer disappears (temperature drops below liquidus everywhere), crystals never exit the two-phase region and the characteristic time for crystal growth is much larger. It takes about 10^9–10^{10} s for the potential temperature to drop from liquidus to the critical temperature for the rheological transition so that the crystals are at least 10 times larger during this period of crystallization

$$d'_{ost} \sim 10^{-2} \text{ m} \qquad (34)$$

8.4. Fractional Versus Equilibrium Crystallization

The above estimates show that the crystal size during the early crystallization of the magma ocean is very close to the critical crystal size separating fractional and equilibrium crystallization of the early magma ocean (Fig. 8). This means that both equilibrium and fractional crystallization (up to 60% crystal fraction) are equally acceptable within the uncertainties of the physical parameters. The potential temperature at which fractional crystallization begins is in the ~300 K interval between the liquidus and the critical temperature for the rheological transition.

9. CRYSTALLIZATION BEYOND RHEOLOGICAL TRANSITION

At the crystal fraction around $\phi_{cr} \sim 60\%$, the melt/crystal mixture undergoes a very sharp rheological transition to a solid-like behavior and the deformation is controlled by the viscosity of the solid phase. Below we will explore what happens beyond this.

Suppose that when the viscosity jumps up to the viscosity of solids the material just stops convecting. A layer with the crystal fraction $\phi \sim \phi_{cr}$ would start accumulating from the bottom of the magma ocean. In about 400 yr (equation (16)), the temperature in the entire magma ocean would

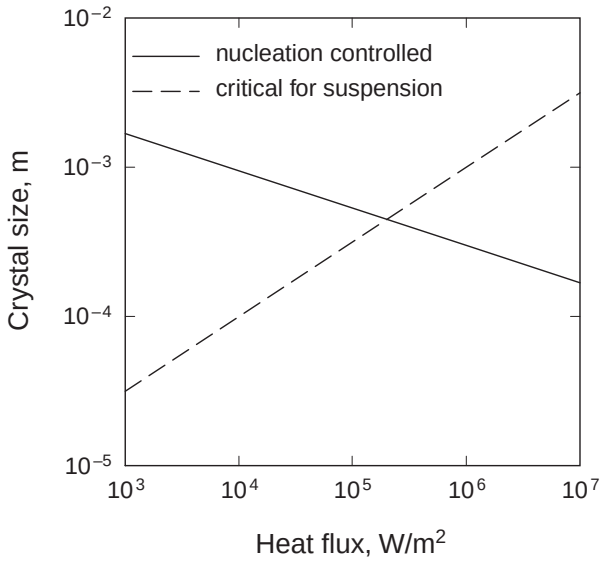

Fig. 8. Crystal size controlled by nucleation (solid line) and the critical crystal size for suspension (dashed line) as functions of the heat flux. The crystal size decreases with the heat flux since the convective velocities, and thus the cooling rates in the descending plumes, increase with the heat flux. On the other hand, the critical crystal size (above which crystals would settle down) increases with the heat flux. The early magma ocean is located near the intersection of these two curves.

approximately follow the curve $\phi = \phi_{cr}$ = const (the dashed line in Fig. 9).

This partially crystallized magma ocean has a huge temperature gradient that follows the curve $\phi = \phi_{cr}$ and therefore is gravitationally unstable. The timescale for Rayleigh-Taylor instability can be estimated from equation (4), in which the effective density difference across the mantle is now $\Delta\rho \approx \rho\alpha\Delta T_{superad}/2$ where $\Delta T_{superad}$ is the superadiabatic temperature contrast across the partially crystallized magma ocean (Fig. 3b).

An important parameter is the viscosity η_s of partially molten rocks. Based on recent estimates of the viscosity in the lower mantle (*Karato and Li*, 1992; *Li et al.*, 1996; *Ita and Cohen*, 1998) the viscosity just above the solidus is expected to be around 10^{18} Pa s for the grain size of about 10^{-3} m. Small amounts of melt reduce the viscosity further. Experimental data suggest that the viscosity is likely to be 1–2 orders of magnitude smaller depending on the melt fraction (*van der Molen and Paterson*, 1979; *Cooper and Kohlstedt*, 1986; *Jin et al.*, 1994; *Rutter and Neumann*, 1995; *Hirth and Kohlstedt*, 1995a,b; *Kohlstedt and Zimmerman*, 1996). For $\eta_s \sim 10^{17}$ Pa s, equation (4) gives $t_{RT} \approx$ 20 yr.

It is clear that the magma ocean would not "wait" for 400 yr until it suddenly "decides" to resolve the instability in 20 yr time. The instability starts developing soon after the critical crystal fraction is reached at the bottom of the magma ocean and takes the form of solid-state convection,

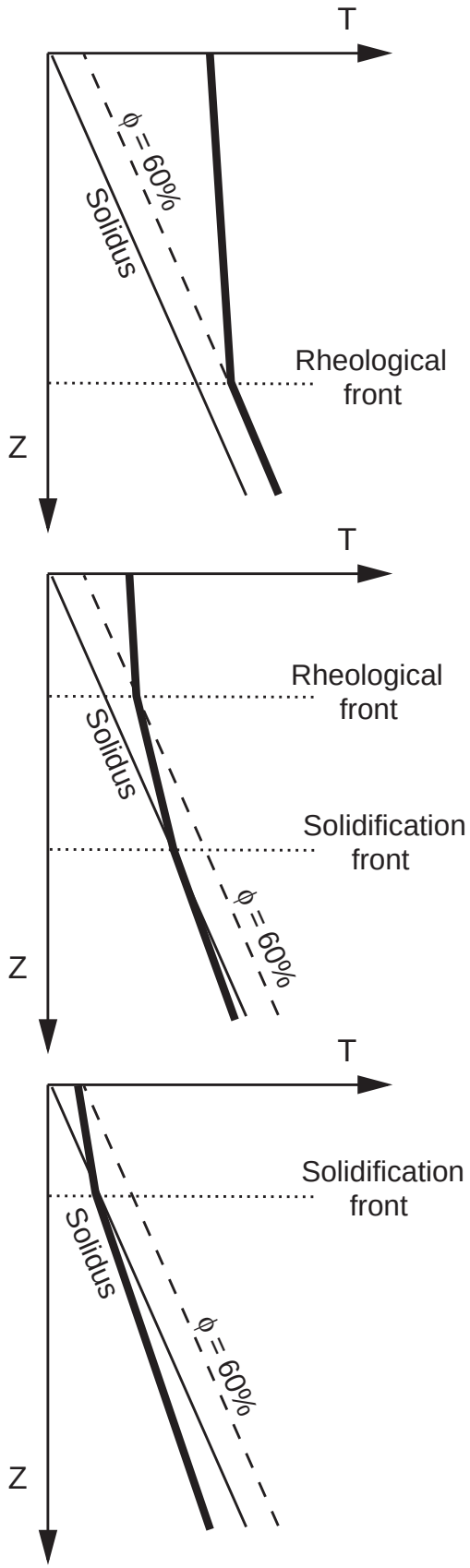

Fig. 9. Propagation of the solidification and rheological fronts in the magma ocean.

which is the primary mechanism of crystallization beyond the critical crystal fraction (*Solomatov and Stevenson,* 1993b). Therefore a complete solidification front would follow the rheological front toward the surface (Fig. 9).

10. DIFFERENTIATION IN THE SHALLOW MAGMA OCEAN

After the rheological front reaches the surface, the driving force for this type of convection motion disappears and it stops. All important changes occur when the potential temperature decreases from liquidus to the critical temperature for the rheological transition. The crystal size becomes larger than the critical one for suspension, the heat flux drops, convection slows down, and a stable crust forms at the surface, reducing further the intensity of convection and the cooling rate of the magma ocean.

The lower bound on the depth $H_{shallow}$ of the remaining shallow magma ocean can be obtained from an adiabat starting at the critical temperature for the rheological transition. Figure 1 suggests that such an adiabat intersects solidus around 10 GPa or $H_{shallow}$ ~300 km. This estimate is rather uncertain since even a 100 K error in the estimate of the rheological transition increases $H_{shallow}$ by a factor of 2. Besides, small superadiabatic gradients can be preserved for a long time and can increase the estimate of $H_{shallow}$ substantially — note that both solidus and liquidus are quite flat between 10 and 23 GPa and even small superadiabatic temperatures can extend the depth of the shallow magma ocean all the way through the bottom of the upper mantle. The presence of water would also increase $H_{shallow}$ although the melt fraction in the temperature range between "dry" solidus and "wet" solidus is small so that "dry" solidus might still be a reasonable basis for defining the depth of the shallow magma ocean.

Moreover, when the potential temperature drops below liquidus, the completely molten layer disappears and the sequence "nucleation-growth-dissolution" changes to just "growth." In this case, the crystals had enough time to reach the critical size for the cessation of suspension (equations (23) and (34)). Although liquidus is only 300 K above the critical temperature for the rheological transition, the bottom of the shallow magma ocean can extend well into the lower mantle, probably around 40 GPa or so (Fig. 3; see also *Miller et al.,* 1991b; *Solomatov and Stevenson,* 1993b; *Abe,* 1997).

Differentiation in the shallow magma ocean takes

$$t_{diff} \sim \frac{H_{shallow}}{u_{perc}} \tag{35}$$

where

$$u_{perc} = \frac{g\Delta\rho d^2\phi_l^2}{150\eta_l(1-\phi_l)} \tag{36}$$

is the percolation velocity according to the Ergun-Orning formula (*Soo,* 1967; *Dullien,* 1979) and ϕ_l is the melt fraction.

For example, it takes

$$t_{diff} \sim 10^8\left(\frac{\phi_l}{0.02}\right)^2\left(\frac{d}{10^{-3}\text{ m}}\right)^2\left(\frac{\eta_l}{100\text{ Pa s}}\right)\text{yr} \tag{37}$$

to reduce the average melt fraction to about 2%. Note that here we used the value of the viscosity of a low-pressure, high-silica, polymerized magma just above the solidus (*Kushiro,* 1980, 1986). Melt/crystal density inversions (*Agee,* 1998) might result in the formation of more than one molten layer. In particular, a gravitationally stable molten layer could be formed at the bottom of the upper mantle in addition to the shallow magma ocean beneath the crust. Cooling and further crystallization of these magmatic layers would take an even longer time depending on the global thermal evolution of the mantle. It can be as fast as 10^7–10^8 yr (*Davies,* 1990). However, if surface recycling was inefficient, convection beneath the solid crust would be slower (e.g., *Solomatov and Moresi,* 1996), and crystallization time would be significantly larger.

11. DISCUSSION AND CONCLUSION

Although the uncertainties in fluid dynamics of magma oceans are substantial, the following scenario of evolution of a terrestrial magma ocean can be suggested.

A giant impact melts a significant part of one hemisphere of the Earth. Isostatic adjustment quickly redistributes the mass to create a more stable spherically symmetric configuration. In the beginning of crystallization of the magma ocean, the temperatures in the deepest parts of the Earth were probably near the solidus and depended on the poorly constrained preimpact thermal state of the mantle. This implies that some portion of the lower mantle could retain substantial amounts of primordial volatiles.

Crystallization starts from the bottom and in less than 1000 yr propagates through the lower mantle. During this period of time, convection can prevent fractionation of crystals up to the critical crystal fraction around 60% (rheological transition from a low-viscosity suspension to a high-viscosity partially molten solid), provided the crystals are smaller than 10^{-3} m. Kinetics of nucleation and crystal growth suggest that this is a possibility. Solid-state convection helps further cooling and crystallization of the partially molten mantle down to the solidus and below. The product of this period of crystallization is essentially undifferentiated mantle with the remaining shallow partially molten layer. This precludes a severe fractionation of minor and trace elements (*Kato et al.,* 1988a,b; *Ringwood,* 1990; *McFarlane and Drake,* 1990; *McFarlane et al.,* 1994). Small amounts of crystals might settle down and contribute to the formation of an Fe-rich D" layer.

The shallow magma ocean is the only part of the mantle that undergoes any substantial differentiation. This can be reconciled with the observed ratios of major and minor el-

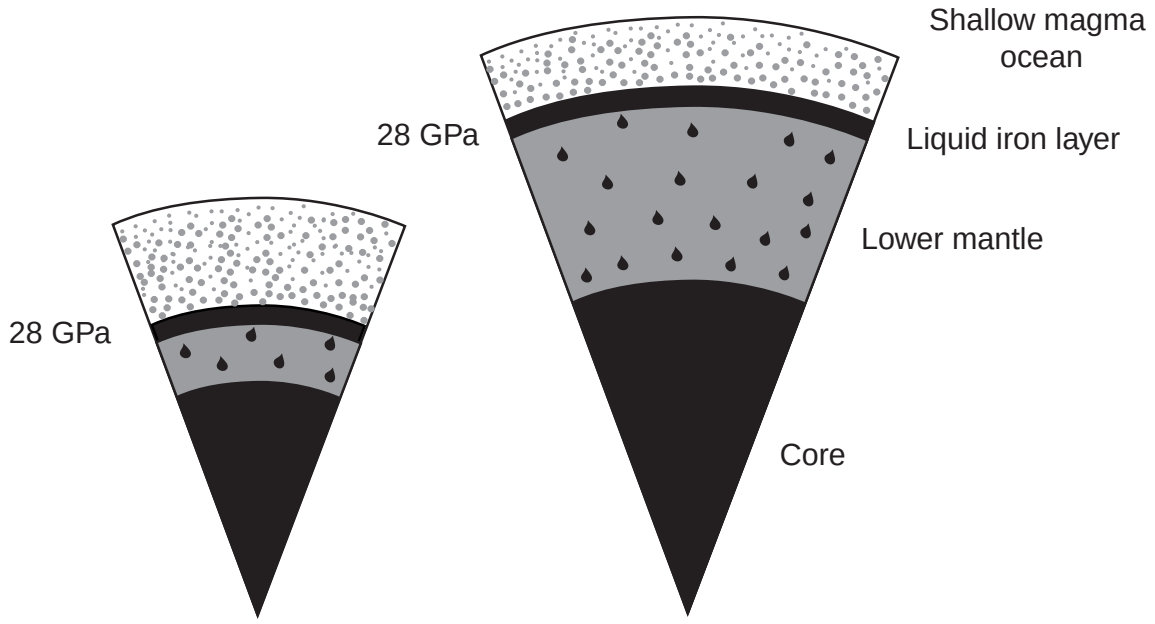

Fig. 10. A possible thermal structure of the growing proto-Earth: a shallow magma ocean where crystal settling/flotation and segregation of liquid Fe delivered by impacts take place; a solid lower mantle with liquid Fe diapirs and a liquid Fe core. The bottom of the shallow magma ocean is located at P = 28 GPa.

ements (*Gasparik and Drake,* 1995). Crystallization of the shallow magma ocean takes more than 10^8 yr and is probably a rather complicated process because of the continuous supply of the new material by meteorites, remelting due to the impacts, and tidal heating (*Sears,* 1993), and a complex pattern of crystal/melt segregation due to crystal/melt density inversions (*Agee,* 1998). This part of the evolution of magma oceans merges with the subsequent thermal evolution of the Earth controlled by radiogenic heating and solid-state convection.

The two very different timescales, 10^3 yr for crystallization of the lower mantle and more than 10^8 yr for crystallization of the shallow magma ocean, suggest that the lower mantle healed very quickly whenever it was molten by a large impact, while the upper mantle never had enough time to crystallize completely. If so, then Fe delivered by impacts accumulated at the boundary of the shallow magma ocean. It formed a gravitationally unstable Fe layer that sank into the Earth's core as discussed by *Elsasser* (1963), *Stevenson* (1981, 1990), and *Karato and Murthy* (1997a,b). These instabilities probably developed in the form of liquid Fe diapirs that were big enough to preclude any significant chemical exchange with the lower mantle (*Stevenson,* 1990; *Karato and Murthy,* 1997a). Therefore chemical equilibrium between Fe and silicates was established at the bottom of this shallow magma ocean (Fig. 10) rather than in the lower mantle (*Tschauner et al.,* 1999).

The sudden drop in the cooling rate of the magma ocean is the factor that determines the location of the bottom of the shallow magma ocean. This happens due to two major events: (1) The potential temperature drops below liquidus so that crystals can grow to much bigger sizes (instead of going through a relatively short "nucleation-growth-dissolution" cycle) and crystal settling/flotation turns off convection; and (2) the potential temperature drops below the critical temperature for the rheological transition (about 60% crystal fraction) at which a large viscosity jump drastically reduces the vigor of convection. The difference in the potential temperature between these two events is only about 300 K, yet the estimates of the corresponding depths of the shallow magma ocean vary from 10 GPa to somewhere around 40 GPa. The experiments on metal/silicate partition coefficients for siderophile elements suggest that chemical equilibrium between liquid Fe and liquid silicate was established at P = 28 GPa (*Li and Agee,* 1996; *Righter et al.,* 1997; *Righter and Drake,* 1997). The bottom of the shallow magma ocean is controlled by pressure rather than by depth. Therefore, it is conceivable that the pressure for metal/silicate equilibrium is the pressure (perhaps an average one) that corresponds to the bottom of the shallow magma ocean.

Many aspects of fluid dynamics of magma oceans remain poorly understood. The structure and evolution of the shallow magma ocean, migration of iron toward the Earth's core, and the effect of water on all processes are among the problems that need to be investigated. It is also clear that the problems of crystallization of magma oceans cannot be separated from other aspects of Earth's formation such as

impacts, core formation, and evolution of the Earth's atmosphere. A self-consistent model of Earth's formation is yet to be developed.

Acknowledgments. This work was supported by NSF grant EAR-9506722, NASA grant NAG5-6897, and the Alfred P. Sloan Foundation. The author thanks K. Righter, F. J. Spera, and D. J. Stevenson for their constructive and thorough reviews.

REFERENCES

Abe Y. (1993) Physical state of the very early Earth. *Lithos, 30,* 223–235.

Abe Y. (1995) Early evolution of the terrestrial planets. *J. Phys. Earth, 43,* 515–535.

Abe Y. (1997) Thermal and chemical evolution of the terrestrial magma ocean. *Phys. Earth Planet. Inter., 100,* 27–39.

Abe Y. and Matsui T. (1986) Early evolution of the Earth: Accretion, atmosphere formation, and thermal history. *Proc. Lunar Planet. Sci. Conf. 17th,* in *J. Geophys. Res., 91,* E291–E302.

Agee C. B. (1990) A new look at differentiation of the Earth from melting experiments on the Allende meteorite. *Nature, 346,* 834–837.

Agee C. B. (1998) Crystal-liquid density inversions in terrestrial and lunar magma oceans. *Phys. Earth Planet. Inter., 107,* 63–74.

Agee C. B. and Walker D. (1988) Mass balance and phase density constraints on early differentiation of chondritic mantle. *Earth Planet. Sci. Lett., 90,* 144–156.

Ahrens T. J. (1992) A magma ocean and the Earth's internal water budget. In *Workshop on the Physics and Chemistry of Magma Oceans from 1 bar to 4 Mbar* (C. B. Agee and J. Longhi, eds.), pp. 5–6. LPI Tech. Rpt. 92-03, Lunar and Planetary Institute, Houston.

Andrade E. N. C. (1952) Viscosity of liquids. *Proc. Roy. Soc. London, A215,* 36–43.

Arzi A. A. (1978) Critical phenomena in the rheology of partially melted rocks. *Tectonophys., 44,* 173–184.

Asimow P. D., Hirschmann M. M., and Stolper E. M. (1997) An analysis of variations in isentropic melt productivity. *Philos. Trans. R. Soc. Lond., A355,* 255–281.

Benz W. and Cameron A. G. W. (1990) Terrestrial effects of the giant impact. In *Origin of the Earth* (H. E. Newsom and J. H. Jones, eds.), pp. 61–67. Oxford Univ., New York.

Benz W., Slattery W. L., and Cameron A. G. W. (1986) The origin of the Moon and the single impact hypothesis, I. *Icarus, 66,* 515–535.

Benz W., Slattery W. L., and Cameron A. G. W. (1987) The origin of the Moon and the single impact hypothesis, II. *Icarus, 71,* 30–45.

Benz W., Cameron A. G. W., and Melosh H. J. (1989) The origin of the Moon and the single impact hypothesis, III. *Icarus, 81,* 113–131.

Boehler R. (1992) Melting of the Fe-FeO and the Fe-FeS systems at high pressure: Constraints on core temperatures. *Earth Planet. Sci. Lett., 111,* 217–227.

Bottinga Y. and Weill D. F. (1972) The viscosity of magmatic silicate liquids: A model for calculation. *Amer. J. Sci., 272,* 438–475.

Bottinga Y., Richet P., and Sipp A. (1995) Viscosity regimes of homogeneous silicate melts. *Amer. Mineral., 80,* 305–318.

Boubnov B. M. and Golitsyn G. S. (1986) Experimental study of convective structures in rotating fluids. *J. Fluid Mech., 167,* 503–531.

Boubnov B. M. and Golitsyn G. S. (1990) Temperature and velocity field regimes of convective motions in a rotating plane fluid layer. *J. Fluid Mech., 219,* 215–239.

Brinkman H. C. (1952) The viscosity of concentrated suspensions and solutions. *J. Chem. Phys., 20,* 571.

Cambell G. A. and Forgacs G. (1990) Viscosity of concentrated suspensions: An approach based on percolation theory. *Phys. Rev., 41A,* 4570–4573.

Cameron A. G. W. (1997) The origin of the Moon and the single impact hypothesis. 5. *Icarus, 126,* 126–137.

Canup R. M. and Agnor C. (2000) Title of chapter. In *Origin of the Earth and Moon* (R. M. Canup and K. Righter, eds.), this volume. Univ. of Arizona, Tucson.

Canup R. M. and Esposito L. W. (1996) Accretion of the Moon from an impact-generated disk. *Icarus, 119,* 427–446.

Cashman K. V. (1993) Relationship between plagioclase crystallization and cooling rate in basaltic melts. *Contrib. Mineral. Petrol., 113,* 126–142.

Castaing B., Gunaratne G., Heslot F., Kadanoff L., Libchaber A., Thomae S., Wu X.-Z., Zaleski S., and Zanetti G. (1989) Scaling of hard thermal turbulence in Rayleigh-Benard convection. *J. Fluid Mech., 204,* 1–30.

Caughey S. J. and Palmer S. G. (1979) Some aspects of turbulence structure through the depth of the convective layer. *Quart. J. R. Met. Soc., 105,* 811–827.

Chen R. H., Fernando J. S., and Boyer D. L. (1989) Formation of isolated vortices in a rotating convecting fluid. *J. Geophys. Res., 94,* 18445–18453.

Cooper R. F. and Kohlstedt D. L. (1986) Rheology and structure of olivine-basalt partial melts. *J. Geophys. Res., 91,* 9315–9323.

Davies G. F. (1982) Ultimate strength of solids and formation of planetary cores. *Geophys. Res. Lett., 11,* 1267–1270.

Davies G. F. (1990) Heat and mass transport in the early Earth. In *Origin of the Earth* (H. E. Newsom and J. H. Jones, eds.), pp. 175–194. Oxford Univ., New York.

Davis M. J., Ihinger P. D., and Lasaga A. C. (1997) Influence of water on nucleation kinetics in silicate melt. *J. Non-Cryst. Solids, 219,* 62–69.

Davis R. H. and Acrivos A. (1985) Sedimentation of noncolloidal particles at low Reynolds numbers. *Annu. Rev. Fluid Mech., 17,* 91–118.

Deardorff J. W. (1970) Convective velocity and temperature scales for the unstable planetary boundary layer and for Rayleigh convection. *J. Atmos. Sci., 27,* 1211–1213.

Dowty E. (1980) Crystal growth and nucleation theory and the numerical simulation of igneous crystallization. In *Physics of Magmatic Processes* (R. V. Hargraves, ed.), pp. 419–485. Princeton Univ., Princeton.

Dullien F. A. L. (1979) *Porous Media: Fluid Transport and Pore Structure.* Academic, San Diego.

Elsasser W. M. (1963) Early history of the Earth. In *Earth Science and Meteorites* (J. Geiss and E. Goldberg, eds.), pp. 1–30. North-Holland, Amsterdam.

Fenn P. M. (1977) The nucleation and growth of alkali feldspars from hydrous melts. *Can. Mineral., 15,* 135–161.

Fernando H. J. S., Chen R. R., and Boyer D. L. (1991) Effects of rotation on convective turbulence. *J. Fluid Mech., 228,* 513–547.

Flasar F. M. and Birch F. (1973) Energetics of core formation: A

correction. *J. Geophys. Res., 78,* 6101–6103.

Flemings M. C., Riek R. G., and Young K. P. (1976) Rheocasting. *Mater. Sci. Eng., 25,* 103–117.

Frankel N. A. and Acrivos A. (1967) On the viscosity of a concentrated suspension of solid spheres. *Chem. Eng. Sci., 22,* 847–853.

Gans R. F. (1972) Viscosity of the Earth's core. *J. Geophys. Res., 77,* 360–366.

Gasparik T. and Drake M. J. (1995) Partitioning of elements among two silicate perovskites, superphase B, and volatile-bearing melt at 23 GPa and 1500–600°C. *Earth Planet. Sci. Lett., 134,* 307–318.

Ghiorso M. S. (1997) Thermodynamic models of igneous processes. *Annu. Rev. Earth Sci., 25,* 221–241.

Glazier J. A., Segawa T., Naert A., and Sano M. (1999) Evidence against 'ultrahard' thermal turbulence at very high Rayleigh numbers. *Nature, 398,* 307–310.

Golitsyn G. S. (1980) Geostrophic convection. *Dokl. Akad. Nauk SSSR, 251,* 1356–1360.

Golitsyn G. S. (1981) Structure of convection in rapid rotation. *Dokl. Akad. Nauk SSSR, 261,* 317–320.

Grossmann S. and Lohse D. (1992) Scaling in hard turbulent Rayleigh-Bénard flow. *Phys. Rev. A, 46,* 903–917.

Grove T. L. (1990) Cooling histories of lavas from Serocki volcano. *Proc. Ocean Drilling Prog., 106/109,* 3–8.

Grove T. L. and Walker D. (1977) Cooling histories of Apollo 15 quartz-normative basalts. *Proc. Lunar Sci. Conf. 8th,* pp. 1501–1520.

Halliday A., Rehkäamper M., Lee D.-C., and Yi W. (1996) Early evolution of the Earth and Moon: New constraints from Hf-W isotope geochemistry. *Earth Planet. Sci. Lett., 142,* 75–89.

Herzberg C. and Gasparik T. (1991) Garnet and pyroxenes in the mantle: A test of the majorite hypothesis. *J. Geophys. Res., 96,* 16263–16274.

Hirth G. and Kohlstedt D. L. (1995a) Experimental constraints on the dynamics of the partially molten upper mantle: Deformation in the diffusion creep regime. *J. Geophys. Res., 100,* 1981–2001.

Hirth G. and Kohlstedt D. L. (1995b) Experimental constraints on the dynamics of the partially molten upper mantle 2. Deformation in the dislocation creep regime. *J. Geophys. Res., 100,* 15441–15449.

Holland K. G. and Ahrens T. J. (1997) Melting of $(Mg,Fe)_2SiO_4$ at the core-mantle boundary of the Earth. *Science, 275,* 1623–1625.

Holloway J. R. (1988) Planetary atmospheres during accretion: The effect of C-O-H-S equilibria (abstract). In *Lunar and Planetary Science XIX,* pp. 499–500. Lunar and Planetary Institute, Houston.

Hopfinger E. J. (1989) Turbulence and vortices in rotating fluids. In *Theoretical and Applied Mechanics* (P. Germain, M. Piau, and D. Caillerie, eds.), pp. 117–138. Elsevier, New York.

Hopfinger E. J., Browand F. K., and Gagne Y. (1982) Turbulence and waves in a rotating tank. *J. Fluid Mech., 125,* 505–534.

Ichikawa K., Kinoshita Y., and Shimamura S. (1985) Grain refinement in Al-Cu binary alloys by rheocasting. *Trans. Japan Inst. Metals, 26,* 513–522.

Ida S., Canup R. M., and Stewart G. R. (1997) Lunar accretion from an impact-generated disk. *Nature, 389,* 353–357.

Ita J. and Cohen R. E. (1998) Diffusion in MgO at high pressure: Implications for lower mantle rheology. *Geophys. Res. Lett., 25,* 1095–1098.

Ito E. and Takahashi E. (1987) Melting of peridotite at uppermost lower-mantle conditions. *Nature, 328,* 514–517.

Jin Z.-M., Green H. W., and Zhou Y. (1994) Melt topology in partially molten mantle peridotite during ductile deformation. *Nature, 372,* 164–167.

Julien K., Legg S., McWilliams J., and Werne J. (1996) Hard turbulence in rotating Rayleigh-Bénard convection. *Phys. Rev. E, 53,* 5557–5560.

Karato S. and Li P. (1992) Diffusion creep in perovskite: Implications for the rheology of the lower mantle. *Science, 255,* 1238–1240.

Karato S.-I. and Murthy V. R. (1997a) Core formation and chemical equilibrium in the Earth — I. Physical consideration. *Phys. Earth Planet. Inter., 100,* 61–79.

Karato S.-I. and Murthy V. R. (1997b) Core formation and chemical equilibrium in the Earth — II. Chemical consequences for the mantle and the core. *Phys. Earth Planet. Inter., 100,* 81–95.

Kashchiev D. (1969) Solution of the nonsteady state problem in nucleation kinetics. *Surf. Sci., 14,* 209–220.

Kasting J. F. (1988) Runaway and moist greenhouse atmosphere and the evolution of Earth and Venus. *Icarus, 74,* 472–494.

Kato T., Ringwood A. E., and Irifune T. (1988a) Experimental determination of element portioning between silicate perovskites, garnets and liquids: Constraints on early differentiation of the mantle. *Earth Planet. Sci. Lett., 89,* 123–145.

Kato T., Ringwood A. E., and Irifune T. (1988b) Constraints on element partition coefficients between $MgSiO_3$ perovskite and liquid determined by direct measurements. *Earth Planet. Sci. Lett., 90,* 65–68.

Kaula W. M. (1979) Thermal evolution of earth and moon growing by planetesimals impacts. *J. Geophys. Res., 84,* 999–1008.

King S. D. (1995) Models of mantle viscosity. In *Mineral Physics and Crystallography: A Handbook of Physical Constants* (T. J. Ahrens, ed.), pp. 227–236. AGU, Washington, DC.

Knittle E. and Jeanloz R. (1989) Melting curve of $(Mg,Fe)SiO_3$ perovskite to 96 GPa: Evidence for a structural transition in lower mantle melts. *Geophys. Res. Lett., 16,* 421–424.

Kohlstedt D. L. and Zimmerman M. E. (1996) Rheology of partially molten mantle rocks. *Annu. Rev. Earth Planet. Sci., 24,* 41–62, 1996.

Kraichnan R. H. (1962) Turbulent thermal convection at arbitrary Prandtl number. *Phys. Fluids, 5,* 1374–1389.

Krieger I. M. and Dougherty T. J. (1959) A mechanism for non-Newtonian flow in suspensions of rigid spheres. *Trans. Soc. Rheol., 3,* 137–152.

Kushiro I. (1980) Viscosity, density, and structure of silicate melts at high pressures, and their petrological applications. In *Physics of Magmatic Processes* (R. B. Hargraves, ed.), pp. 93–120. Princeton Univ., Princeton.

Kushiro I. (1986) Viscosity of partial melts in the upper mantle. *J. Geophys. Res., 91,* 9343–9350.

Lee D.-C. and Halliday A. N. (1995) Hafnium-tungsten chronometry and the timing of terrestrial core formation. *Nature, 378,* 771–774.

Lejeune A.-M. and Richet P. (1995) Rheology of crystal-bearing silicate melts: An experimental study at high viscosities. *J. Geophys. Res., 100,* 4215–4229.

Li. J. and Agee C. B. (1996) Geochemistry of mantle-core differentiation at high pressure. *Nature, 381,* 686–689.

Lifshitz I. M. and Slyozov V. V. (1961) The kinetics of precipitation from supersaturated solid solution. *J. Phys. Chem. Solids, 19,* 35–50.

Li P., Karato S., and Wang Z. (1996) High-temperature creep in

fine-grained polycrystalline $CaTiO_3$, an analogue material of $(Mg,Fe)SiO_3$. *Phys. Earth Planet. Inter., 95,* 19–36.

Lofgren G., Donaldson C. H., Williams R. J., Mullins O., and Usselman T. M. (1974) Experimentally reproduced textures and mineral chemistry of Apollo 15 quartz-normative basalts. *Proc. Lunar Sci. Conf. 5th,* pp. 549–567.

Martin D. and Nokes R. (1988) Crystal settling in a vigorously convecting magma chamber. *Nature, 332,* 534–536.

Martin D. and Nokes R. (1989) A fluid dynamical study of crystal settling in convecting magmas. *J. Petrol., 30,* 1471–1500.

Matsui T. and Abe Y. (1986) Formation of a "magma ocean" on the terrestrial planets due to the blanketing effect of an impact-induced atmosphere. *Earth Moon Planets, 34,* 223–230.

McBirney A. R. and Murase T. (1984) Rheological properties of magmas. *Annu. Rev. Earth Planet. Sci., 12,* 337–357.

McFarlane E. A. and Drake M. J. (1990) Element partitioning and the early thermal history of the Earth. In *Origin of the Earth* (H. E. Newsom and J. H. Jones, eds.), pp. 135–150. Oxford Univ., New York.

McFarlane E. A., Drake M. J., and Rubie D. C. (1994) Element partitioning between Mg-perovskite, magnesiowüstite, and silicate melt at conditions of the Earth's mantle. *Geochim. Cosmochim. Acta, 58,* 5161–5172.

McKenzie D. and Bickle M. J. (1988) The volume and composition of melt generated by extension of the lithosphere. *J. Petrol., 29,* 625–679.

Melosh H. J. (1990) Giant impacts and thermal state of the early Earth. In *Origin of the Earth* (H. E. Newsom and J. H. Jones, eds.), pp. 69–83. Oxford Univ., New York.

Miller G. H., Stolper E. M., and Ahrens T. J. (1991a) The equation of state of a molten komatiite, 1, Shock wave compression to 36 GPa. *J. Geophys. Res., 96,* 11831–11848.

Miller G. H., Stolper E. M., and Ahrens T. J. (1991b) The equation of state of a molten komatiite, 2, Application to komatiite petrogenesis and the Hadean mantle. *J. Geophys. Res., 96,* 11849–11864.

Mooney M. (1951) The viscosity of a concentrated suspension of spherical particles. *J. Colloid. Sci., 6,* 162–170.

Murray J. D. (1965) On the mathematics of fluidization, Part I, Fundamental equations and wave propagation. *J. Fluid Mech., 21,* 465–493.

Newsom H. E. and Taylor S. R. (1989) Geochemical implications of the formation of the Moon by a single great impact. *Nature, 338,* 29–34.

Ohtani E. (1985) The primordial terrestrial magma ocean and its implication for stratification of the mantle. *Phys. Earth Planet. Inter., 38,* 70–80.

Ohtani E. and Sawamoto H. (1987) Melting experiment on a model chondritic mantle composition at 25 GPa. *Geophys. Res. Lett., 14,* 733–736.

Persikov E. S., Zharikov V. A., Bukhtiyarov P. G., and Polskoy S. F. (1990) The effect of volatiles on the properties of magmatic melts. *Eur. J. Mineral., 2,* 621–642.

Pierazzo E., Vickery A. M., and Melosh H. J. (1997) A reevaluation of impact melt production. *Icarus, 127,* 408–423.

Presnall D. C., Weng Y.-H., Milholland C. S., and Walter M. J. (1998) Liquidus phase relations in the system MgO-$MgSiO_3$ at pressures up to 25 GPa — constraints on crystallization of a Hadean mantle. *Phys. Earth Planet. Inter., 107,* 83–95.

Priestly C. H. B. (1959) *Turbulent Transfer in the Lower Atmosphere.* Univ. of Chicago, Chicago.

Righter K. and Drake M. J. (1997) Metal-silicate equilibrium in a homogeneously accreting Earth: New results for Re. *Earth Planet. Sci. Lett., 146,* 541–553.

Righter K., Drake M. J., and Yaxley G. (1997) Prediction of siderophile element metal-silicate partition coefficients to 20 GPa and 2800°C: The effects of pressure, temperature, oxygen fugacity, and silicate and metallic melt compositions. *Phys. Earth Planet. Inter., 100,* 115–134.

Ringwood A. E. (1990) Earliest history of the Earth-Moon system. In *Origin of the Earth* (H. E. Newsom and J. H. Jones, eds.), pp. 101–134. Oxford Univ., New York.

Roscoe R. (1952) The viscosity of suspensions of rigid spheres. *Brit. J. Appl. Phys., 3,* 267–269.

Rutter E. H. and Neumann D. H. K. (1995) Experimental deformation of partially molten Westerly granite under fluid-absent conditions, with implications for the extraction of granitic magmas. *J. Geophys. Res., 100,* 15697–15715.

Safronov V. S. (1978) The heating of the Earth during its formation. *Icarus, 33,* 3–12.

Sasaki S. and Nakazawa K. (1986) Metal-silicate fractionation in the growing Earth: Energy source for the terrestrial magma ocean. *J. Geophys. Res., 91,* 9231–9238.

Shaw H. R. (1972) Viscosities of magmatic silicate liquids: An empirical method of prediction. *Am. J. Sci., 272,* 870–893.

Scarfe C. M. and Takahashi E. (1986) Melting of garnet peridotite to 13 GPa and the early history of the upper mantle. *Nature, 322,* 354–356.

Sears W. D. (1993) Tidal dissipation and the giant impact origin for the Moon (abstract). In *Lunar and Planetary Science XXIII,* pp. 1255–1256. Lunar and Planetary Institute, Houston.

Shraiman B. I. and Siggia E. D. (1990) Heat transport in high-Rayleigh-number convection. *Phys. Rev. A, 42,* 3650–3653.

Siggia E. D. (1994) High Rayleigh number convection. *Annu. Rev. Fluid Mech., 26,* 137–168.

Smith D. M., Eady J. A., Hogan L. M., and Irwin D. W. (1991) Crystallization of a faceted primary phase in a stirred slurry. *Metall. Trans., 22A,* 575–584.

Solomatov V. S. (1995) Batch crystallization under continuous cooling: Analytical solution for diffusion limited crystal growth. *J. Crystal Growth, 148,* 421–431.

Solomatov V. S. and Moresi L.-N. (1996) Stagnant lid convection on Venus. *J. Geophys. Res., 101,* 4737–4753.

Solomatov V. S. and Stevenson D. J. (1993a) Suspension in convective layers and style of differentiation of a terrestrial magma ocean. *J. Geophys. Res., 98,* 5375–5390.

Solomatov V. S. and Stevenson D. J. (1993b) Nonfractional crystallization of a terrestrial magma ocean. *J. Geophys. Res., 98,* 5391–5406.

Solomatov V. S. and Stevenson D. J. (1993c) Kinetics of crystal growth in a terrestrial magma ocean. *J. Geophys. Res., 98,* 5407–5418.

Solomatov V. S., Olson P., and Stevenson D. J. (1993) Entrainment from a bed of particles by thermal convection. *Earth Planet. Sci. Lett., 120,* 387–393.

Soo S. L. (1967) *Fluid Dynamics of Multiphase Systems.* Blaisdell, Waltham. 524 pp.

Spera F. J. (1992) Lunar magma transport phenomena. *Geochim. Cosmochim. Acta, 56,* 2253–2265.

Stevenson D. J. (1981) Models of the Earth's core. *Science, 214,* 611–619.

Stevenson D. J. (1987) Origin of the Moon — The collision hypothesis. *Annu. Rev. Earth Planet. Sci., 15,* 271–315.

Stevenson D. J. (1990) Fluid dynamics of core formation. In *Origin of the Earth* (H. E. Newsom and J. H. Jones, eds.), pp. 231–249. Oxford Univ., New York.

Stishov S. M. (1988) Entropy, disorder, melting. *Sov. Phys. Uspekhi, 31,* 52–67.

Swanson S. E. (1977) Relation of nucleation and crystal-growth rate to the development of granitic textures. *Amer. Mineral., 62,* 966–978.

Thompson C. and Stevenson D. J. (1988) Gravitational instabilities in 2-phase disks and the origin of the Moon. *Astrophys. J., 333,* 452–481.

Tonks W. B. and Melosh H. J. (1990) The physics of crystal settling and suspension in a turbulent magma ocean. In *Origin of the Earth* (H. E. Newsom and J. H. Jones, eds.), pp. 151–174. Oxford Univ., New York.

Tonks W. B. and Melosh H. J. (1992) Core formation by giant impacts. *Icarus, 100,* 326–346.

Tonks W. B. and Melosh H. J. (1993) Magma ocean formation due to giant impacts. *J. Geophys. Res., 98,* 5319–5333.

Turcotte D. L. and Schubert G. (1982) *Geodynamics: Applications of Continuum Physics to Geological Problems.* Wiley, New York.

Tschauner O., Zerr A., Specht S., Rocholl A., Boehler R., and Palme H. (1999) Partitioning of nickel and cobalt between silicate perovskite and metal at pressures up to 80 GPa. *Nature, 398,* 604–607.

van der Molen I. and Paterson M. S. (1979) Experimental deformation of partially-melted granite. *Contrib. Mineral. Petrol., 70,* 299–318.

Voorhees P. W. (1992) Ostwald ripening of two-phase mixtures. *Annu. Rev. Mater. Sci., 22,* 197–215.

Walker D., Powell M. A., Lofgren G. E., and Hays J. F. (1978) Dynamic crystallization of a eucrite basalt. *Proc. Lunar Planet. Sci. Conf. 9th,* pp. 1369–1391.

Wasserman E. A., Yuen D. A., and Rustad J. R. (1993a) Compositional effects on the transport and thermodynamic properties of MgO-SiO_2 mixtures using molecular dynamics. *Phys. Earth Planet. Inter., 77,* 189–203.

Wasserman E. A., Yuen D. A., and Rustad J. R. (1993b) Molecular dynamics study of the transport properties of perovskite melts under high-temperature and pressure conditions. *Earth Planet. Sci. Lett., 114,* 373–384.

Weidenschilling S. J., Spaute D., Davis D. R., Marzari F., and Ohtsuki K. (1997) Accretional evolution of a planetesimal swarm. 2. The terrestrial zone. *Icarus, 126,* 429–455.

Wetherill G. W. (1985) Occurrence of giant impacts during the growth of the terrestrial planets. *Science, 228,* 877–879.

Wetherill G. W. (1990) Formation of the Earth. *Annu. Rev. Earth Planet. Sci., 18,* 205–256.

Willis G. E. and Deardorff J. W. (1974) A laboratory model of the unstable planetary boundary layer. *J. Atmos. Sci., 31,* 1297–1307.

Zahnle K. J., Kasting J. F., and Pollack J. B. (1988) Evolution of a steam atmosphere during Earth's accretion. *Icarus, 74,* 62–97.

Zerr A. and Boehler R. (1993) Melting of (Mg,Fe)SiO_3-perovskite to 625 kilobars: Indication of a high melting temperature in the lower mantle. *Science, 262,* 553–557.

Zerr A. and Boehler R. (1994) Constraints on the melting temperature of the lower mantle from high-pressure experiments on MgO and magnesiowüstite. *Nature, 371,* 506–508.

Zerr A., Diegeler A., and Boehler R. (1998) Solidus of Earth's deep mantle. *Science, 281,* 243–246.

Zhang J. and Herzberg C. T. (1994) Melting experiments on anhydrous peridotite KLB-1 from 5.0 to 22.5 GPa. *J. Geophys. Res., 99,* 17729–17742.